The Astrophysical Journal Letters, 892:L15 (6pp), 2020 March 20 https://doi.org/10.3847/2041-8213/ab7cdd

Periodic Fast Radio Bursts with Neutron Star Free Precession

J. J. Zanazzi[1] and Dong Lai[2,3]
[1] Canadian Institute for Theoretical Astrophysics, University of Toronto, 60 St. George Street, Toronto, ON M5S 1A7, Canada; jzanazzi@cita.utoronto.ca
[2] Department of Astronomy, Center for Astrophysics and Planetary Science, Cornell University, Ithaca, NY 14853, USA
[3] Department of Astronomy and Miller Institute for Basic Research In Science, UC Berkeley, Berkeley, CA 94720, USA
Received 2020 February 13; revised 2020 March 4; accepted 2020 March 4; published 2020 March 25

Abstract

The CHIME/FRB collaboration recently reported the detection of a 16 day periodicity in the arrival times of radio bursts from FRB 180916.J0158+65. We study the possibility that the observed periodicity arises from free precession of a magnetized neutron star, and put constraints on different components of the star's magnetic fields. Using a simple geometric model, where radio bursts are emitted from a rotating neutron star magnetosphere, we show that the emission pattern as a function of time can match that observed from FRB 180916.J0158+65.

Unified Astronomy Thesaurus concepts: Compact radiation sources (289); Magnetospheric radio emissions (998); Radio bursts (1339); Neutron stars (1108); Magnetars (992)

1. Introduction

Fast radio bursts (FRBs) are extragalactic millisecond radio transients, and their origin is mysterious (Katz 2018a; Cordes & Chatterjee 2019; Petroff et al. 2019). An increasing number of FRBs have been found to repeat (CHIME/FRB Collaboration et al. 2019). So far, no sign of periodicity has been detected in any FRBs (such as FRB 121101; Katz 2018b; Zhang et al. 2018). Recently, the Canadian Hydrogen Intensity Mapping Experiment Fast Radio Burst Project (CHIME/FRB) team reported the detection of periodicity from a repeating FRB 180916.J0158+65 (hereafter FRB 180916; The CHIME/FRB Collaboration et al. 2020): the 28 bursts recorded by CHIME in the 410 day time span (from 2018 September to 2019 October) exhibit a period of 16.35 ± 0.18 days in arrival times, and cluster in a $\sim$4 day phase window. This finding, if confirmed by future observations and found to be generic for many FRBs, would provide a significant clue to the nature of these objects.

The CHIME discovery paper already discussed several possible origins for the periodicity, including pulsars in binaries and isolated precessing neutron stars. In this Letter we examine the latter possibility and the implication for the central engine of FRBs (see also Levin et al. 2020).

Neutron star (NS) precession has long been studied in the literature. It was recognized early on that superfluid vortex pinning in the NS crust suppresses free precession (Shaham 1977). Revised superfluid properties or the absence of superfluidity may still allow precession to occur (Link & Epstein 1997; Sedrakian et al. 1999; Akgün et al. 2006; Goglichidze & Barsukov 2019). Some observed long-term variabilities of radio pulsar emission (Kramer et al. 2006; Weisberg et al. 2010; Lyne et al. 2013) may be attributed to free precession (Zanazzi & Lai 2015; Arzamasskiy et al. 2015). Free precession could also influence the X-ray variability and spin-down of magnetars in the Galaxy (Melatos 1999).

This work investigates if NS free precession can explain the periodicity of FRB 180916. In Section 2 we constrain NS magnetic fields from the observed period, and calculate the emission pattern from a simple geometrical FRB model. We discuss the effect of precession on linear polarization in Section 3 and conclude in Section 4.

2. Periodic FRBs from NS Precession

2.1. Free Precession of NS

Consider an NS with mass M, radius R, dipolar magnetic field of strength $B_{\rm p}$, dipole moment $p = \frac{1}{2}B_{\rm p}R^3$ and axis $\hat{\boldsymbol{p}}$, spin period P, and spin frequency $\omega = 2\pi/P$. The NS could also have complex quadrupole field and internal fields (see below). For simplicity, we assume the NS is homogeneous, with a constant density $\rho = 3M/(4\pi R^3)$ and moment of inertia $I = \frac{2}{5}MR^2$. We define $\bar{R}_6 = R/(10^6\ {\rm cm})$ and $\bar{M}_{1.4} = M/(1.4\,M_\odot)$.

In the frame rotating with the NS, the equations of motion describing the evolution of the NS spin vector $\boldsymbol{\omega} = \omega\hat{\boldsymbol{\omega}}$ is (Zanazzi & Lai 2015)

$$\frac{{\rm d}\boldsymbol{L}_{\rm eff}}{{\rm d}t} + \boldsymbol{\omega} \times \boldsymbol{L}_{\rm eff} = 0, \tag{1}$$

where $\boldsymbol{L}_{\rm eff} = \boldsymbol{I}_{\rm eff} \cdot \boldsymbol{\omega}$ is the effective angular momentum of the NS. The effective moment of inertia tensor $\boldsymbol{I}_{\rm eff}$ takes account of the nonsphericity of the NS due to rotation and internal magnetic fields, as well as the inertia from the near-zone fields corotating with the NS (Davis & Goldstein 1970; Goldreich 1970; Zanazzi & Lai 2015). Take I_i to be the eigenvalues of $\boldsymbol{I}_{\rm eff}$ (effective principal moments of inertia), with $\hat{\boldsymbol{I}}_i$ their associated unit eigenvectors (effective principal axes). For simplicity, we assume $I_1 = I_2$, but $\epsilon_{\rm eff} = (I_3 - I_1)/I_1 \neq 0$ (biaxial NS; we assume $|\epsilon_{\rm eff}| \ll 1$ throughout). Then Equation (1) has the solution (Landau & Lifshitz 1969; Goldreich 1970)

$$\hat{\boldsymbol{\omega}} = \sin\theta\cos\varphi_\omega\hat{\boldsymbol{I}}_1 + \sin\theta\sin\varphi_\omega\hat{\boldsymbol{I}}_2 + \cos\theta\hat{\boldsymbol{I}}_3, \tag{2}$$

where

$$\varphi_\omega(t) = (\epsilon_{\rm eff}\,\omega\cos\theta)t + \varphi_{\omega 0} \tag{3}$$

is the precession phase of $\hat{\boldsymbol{\omega}}$ around $\hat{\boldsymbol{I}}_3$, with $\varphi_{\omega 0} = \varphi_\omega(0)$, while θ is the angle between $\hat{\boldsymbol{\omega}}$ and $\hat{\boldsymbol{I}}_3$ ($\cos\theta = \hat{\boldsymbol{\omega}} \cdot \hat{\boldsymbol{I}}_3$). Notice ω and θ are constants of motion for Equation (1). The NS precession

period $P_{\rm prec}$ is then

$$P_{\rm prec} = \frac{P}{\epsilon_{\rm eff}\cos\theta}. \tag{4}$$

When $I_1 \neq I_2$, Equation (1) can be solved with qualitatively similar dynamics, except the magnitude of ω oscillates and θ nutates with time (Landau & Lifshitz 1969; Melatos 1999; Zanazzi & Lai 2015; see also Levin et al. 2020 for why triaxiality does not make the precession rate vary for a nearly spherical rotator).

We postulate that the observed 16.35 day period seen in FRB 180916 is the precession period $P_{\rm prec}$. This constrains $\epsilon_{\rm eff}$ to be

$$\epsilon_{\rm eff} = \frac{7.1\times10^{-7}}{\cos\theta}\left(\frac{P}{1\ {\rm s}}\right)\left(\frac{16.35\ {\rm days}}{P_{\rm prec}}\right). \tag{5}$$

There are several contributions to the nonsphericity parameter $\epsilon_{\rm eff}$. Two primary sources are intrinsic to the NS. The first arises from the internal magnetic field of strength $B_\star$, leading to a deformation of order

$$\epsilon_{\rm mag} = \beta\frac{R^4B_\star^2}{GM^2} = 1.9\times10^{-6}\beta\left(\frac{B_\star}{10^{15}\ {\rm G}}\right)^2\frac{\bar{R}_6^4}{\bar{M}_{1.4}^2}, \tag{6}$$

where β is a constant satisfying $|\beta| \ll 1$ (either $\beta > 0$ or $\beta < 0$), with a value that depends on the magnetic field's topology (Mastrano et al. 2013); a complex internal field can yield $|\beta| \ll 1$. The second deformation source is an elastic crust that has a rotational bulge with principal axis $\hat{\boldsymbol{I}}_3$ misaligned with $\hat{\boldsymbol{\omega}}$, formed when the crust crystallized at a higher rotational frequency (e.g., Goldreich 1970; Cutler et al. 2003). Assuming the NS has a uniform shear modulus μ, the deformation from elasticity is of order (assuming $19\mu \ll 2\rho gR$, where $g = GM/R^2$; Munk & MacDonald 1975)

$$\begin{aligned}\epsilon_{\rm elast} &\simeq \left(\frac{19\mu}{2\rho gR}\right)\left(\frac{15\omega^2}{16\pi G\rho}\right)\\ &= 2.0\times10^{-11}\left(\frac{\mu}{10^{30}\ {\rm dynes\ cm^{-2}}}\right)\left(\frac{1\ {\rm s}}{P}\right)^2\frac{\bar{R}_6^7}{\bar{M}_{1.4}^3}.\end{aligned} \tag{7}$$

Although the frozen-in rotational deformation could be larger when the NS was born rotating fast, the NS's spin-down causes the crust to experience stress and break before the NS has slowed to near its present rotation rate (e.g., Baym & Pines 1971; Cutler et al. 2003). Since the NS may have experienced many crust-quakes over its lifetime, it is reasonable to assume that the frozen-in rotational deformation is of order the present rotational deformation.

In addition to the intrinsic deformations $\epsilon_{\rm mag}$ and $\epsilon_{\rm elast}$, the near-zone fields corotating with the NS induce a precessional torque (Goldreich 1970), and this effect can be incorporated into the effective deformation parameter (Zanazzi & Lai 2015). The dipole field gives (Melatos 1999, 2000; Zanazzi & Lai 2015)

$$\epsilon_{\rm p} = \frac{3B_{\rm p}^2R^5}{20Ic^2} = 1.5\times10^{-7}\left(\frac{B_{\rm p}}{10^{15}\ {\rm G}}\right)^2\frac{\bar{R}_6^3}{\bar{M}_{1.4}}. \tag{8}$$

Equation (8) takes into account the inertia of the field exterior to the NS in vacuum; including the inertia of the field inside the NS (Beskin & Zheltoukhov 2014), or the effect of magnetosphere plasma (Arzamasskiy et al. 2015), modifies Equation (8) by factors of order unity. Similarly, a quadrupolar magnetic field with strengths specified by $B_\parallel$ and B_δ leads to deformations of order

$$\epsilon_\parallel = \frac{4}{105}\left(\frac{B_\parallel}{B_{\rm p}}\right)^2\epsilon_{\rm p}, \qquad \epsilon_\delta = \frac{16}{945}\left(\frac{B_\delta}{B_{\rm p}}\right)^2\epsilon_{\rm p}; \tag{9}$$

see Zanazzi & Lai (2015) for details and definitions of $B_\parallel$ and B_δ. For magnetic field strengths ($B \sim 10^{15}$ G) and spin periods ($P \sim 1$ s) typical of magnetars, we see $\epsilon_{\rm mag}$, $\epsilon_{\rm p}$, $\epsilon_\parallel$, and ϵ_δ are all feasible ways to effectively deform the NS to give a spin precession period $P_{\rm prec} = 16.35$ days, but elastic deformation $\epsilon_{\rm elast}$ requires $P \sim 1$ ms to get $\epsilon_{\rm elast} \sim \epsilon_{\rm eff}$. Since this is much shorter than a typical magnetar P value, we will not consider $\epsilon_{\rm elast}$ for the remainder of this work.

In Equation (1), we have neglected the radiative torque, which works to spin down the NS and secularly align $\hat{\boldsymbol{\omega}}$ with $\hat{\boldsymbol{p}}$. This is valid as long as the shift in the NS precession phase due to spin-down over the course of the observation ($\Delta\varphi_\omega \sim 2\pi t_{\rm obs}^2/[P_{\rm prec}t_{\rm sd}]$) is less than unity, where

$$t_{\rm sd} = \frac{3c^3I}{2p^2\omega^2} = 145\left(\frac{P}{1\ {\rm s}}\right)^2\left(\frac{10^{15}\ {\rm G}}{B_{\rm p}}\right)^2\frac{\bar{M}_{1.4}}{\bar{R}_6^4}\ {\rm yr} \tag{10}$$

is the spin-down time for the NS, and $t_{\rm obs} = 410$ days is the length of time that FRB 180916 was observed. Requiring $\Delta\varphi_\omega \lesssim 1$ gives the constraint $t_{\rm sd} \gtrsim 2\pi t_{\rm obs}^2/P_{\rm prec} \equiv t_{\rm sd,min}$ for our precession model.[4]

Figure 1 depicts the constraints on the NS spin period P and the strengths of various magnetic field components (internal, dipole, and quadrupole) in order for magnetic deformations (both intrinsic and effective) to produce $P_{\rm prec} = 16.35$ days. For spin periods $P \sim 0.1 - 10$ s, a range of magnetic field values ($B \sim 10^{14} - 10^{17}$) are required, depending on which deformation mechanism dominates $\epsilon_{\rm eff}$. Figure 1 also shows the condition $t_{\rm sd} = t_{\rm sd,min}$. For the NS to stably precess over the observed duration of FRB 180916 ($t_{\rm obs}$) with a given poloidal field $B_{\rm p}$, the P value must lie somewhat above the red line.

Over timescales comparable to $t_{\rm sd}$, the NS spin frequency ω and precession angle θ evolve due to the radiative torque. When $t_{\rm sd} \gg P_{\rm prec}$, the evolutionary equations for ω and θ are (Goldreich 1970; Zanazzi & Lai 2015)

$$\frac{{\rm d}\omega}{{\rm d}t} = -\frac{\omega}{t_{\rm sd}}\left[\sin^2\psi + \sin^2\theta\left(1 - \frac{3}{2}\sin^2\psi\right)\right], \tag{11}$$

$$\frac{{\rm d}\theta}{{\rm d}t} = -\frac{1}{t_{\rm sd}}\cos\theta\sin\theta\left(1 - \frac{3}{2}\sin^2\psi\right). \tag{12}$$

Figure 2 depicts an example of the evolution of P, θ, $P_{\rm prec}$, and χ (the magnetic inclination angle, or angle between $\hat{\boldsymbol{\omega}}$ and the dipole axis $\hat{\boldsymbol{p}}$) over timescales comparable to $t_{\rm sd}$. For the example given, P and $P_{\rm prec}$ increase, while θ and χ decrease, with time.

2.2. Model for FRB Emission from Precessing NS

The central engine of FRBs and the radiation mechanism are uncertain. Given the millisecond timescale of the radio bursts, it is natural that most models associate FRB emissions to

[4] Note that the precession period is always less than $t_{\rm sd}$ by a factor $\lesssim \omega R/c$, since $\epsilon_{\rm eff} \gtrsim \epsilon_{\rm p}$, and thus $P_{\rm prec} \lesssim P/\epsilon_{\rm p} \sim (\omega R/c)t_{\rm sd}$.

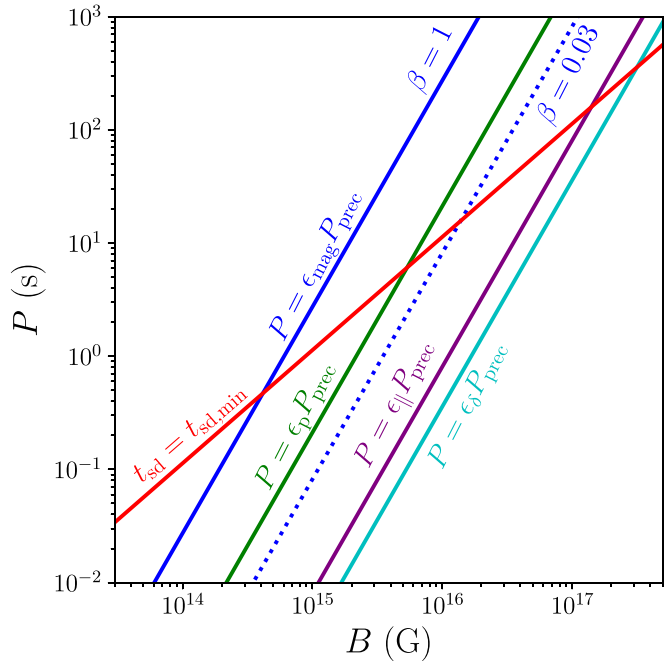

Figure 1. NS spin period P and magnetic field strength B that lead to a spin precession period $P_{\rm prec} = 16.35$ days (Equation (4)), with the effective ellipticity $\epsilon_{\rm eff} = \epsilon_{\rm mag}$ (blue; Equation (6) with $B = B_\star$), $\epsilon_{\rm eff} = \epsilon_{\rm p}$ (green; Equation (8) with $B = B_{\rm p}$), $\epsilon_{\rm eff} = \epsilon_{\parallel}$ (purple; Equation (9) with $B = B_{\parallel}$), and $\epsilon_{\rm eff} = \epsilon_{\delta}$ (cyan; Equation (9) with $B = B_{\delta}$). The red line displays the P and $B = B_{\rm p}$ values when the duration over which FRB 180916 was observed ($t_{\rm obs} = 410$ days) equals the NS spin-down time $t_{\rm sd}$ (Equation (10)). Here, $\cos\theta = 1$, with $\beta = 1$ (solid) and $\beta = 0.03$ (dotted).

magnetized neutron stars (e.g., Lyubarsky 2014; Cordes & Wasserman 2016; Katz 2016; Beloborodov 2017; Lu & Kumar 2018; Margalit et al. 2019). Here we consider a simple geometric model to illustrate how NS precession affects the arrival times of radio bursts from NSs. We use the terminology "arrival times" for FRB emission in our model, but note there are no propagation effects.

Figure 3 presents the setup for our emission model, in the frame corotating with the NS (body frame), with (effective) principal axis $\hat{\boldsymbol{I}}_i$ defining an orthogonal coordinate system. The NS spin axis $\hat{\boldsymbol{\omega}}$ is inclined to $\hat{\boldsymbol{I}}_3$ by an angle θ ($\cos\theta = \hat{\boldsymbol{\omega}} \cdot \hat{\boldsymbol{I}}_3$), and precesses about $\hat{\boldsymbol{I}}_3$ at the period $P_{\rm prec}$ (Equation (4); see Equation (2)). An observer views the NS in a direction $\hat{\boldsymbol{n}}$ constant in the inertial frame, but rotating about $\hat{\boldsymbol{\omega}}$ in the body frame with inclination ν ($\cos\nu = \hat{\boldsymbol{n}} \cdot \hat{\boldsymbol{\omega}}$) and spin period P. Note that in the body frame of the NS, $\hat{\boldsymbol{n}}$ satisfies the equation $\mathrm{d}\hat{\boldsymbol{n}}/\mathrm{d}t + \boldsymbol{\omega} \times \hat{\boldsymbol{n}} = 0$. Since $\hat{\boldsymbol{\omega}}$ evolves over a timescale much longer than $\hat{\boldsymbol{n}}$ ($|\mathrm{d}\hat{\boldsymbol{\omega}}/\mathrm{d}t|/|\mathrm{d}\hat{\boldsymbol{n}}/\mathrm{d}t| \sim \epsilon_{\rm eff} \ll 1$), we can treat $\hat{\boldsymbol{\omega}}$ as approximately constant to obtain

$$\hat{\boldsymbol{n}}(t) = \frac{\sin\nu\cos\varphi_n}{\sin\theta}(\hat{\boldsymbol{I}}_3 \times \hat{\boldsymbol{\omega}}) \times \hat{\boldsymbol{\omega}} - \frac{\sin\nu\sin\varphi_n}{\sin\theta}(\hat{\boldsymbol{I}}_3 \times \hat{\boldsymbol{\omega}}) + (\cos\nu)\hat{\boldsymbol{\omega}}, \quad (13)$$

where

$$\varphi_n(t) = \omega t + \varphi_{n0} \quad (14)$$

is the rotation phase of $\hat{\boldsymbol{n}}$ around $\hat{\boldsymbol{\omega}}$, with $\varphi_{n0} = \varphi_n(0)$. The NS's dipole axis $\hat{\boldsymbol{p}}$ is fixed in the body frame, inclined to $\hat{\boldsymbol{I}}_3$ by an angle ψ ($\cos\psi = \hat{\boldsymbol{p}} \cdot \hat{\boldsymbol{I}}_3$). For concreteness, we take $\hat{\boldsymbol{p}}$ to lie in

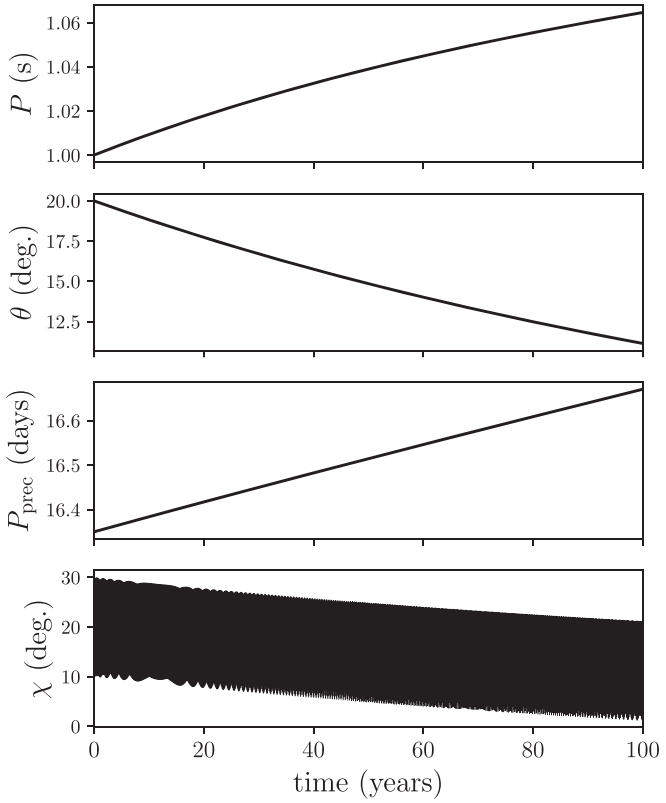

Figure 2. Time evolution of the NS spin period P (first panel), precession angle θ (second panel; see Figure 3), precession period $P_{\rm prec}$ (third panel; Equation (4)), and magnetic inclination angle χ (last panel; angle between $\hat{\boldsymbol{p}}$ and $\hat{\boldsymbol{\omega}}$). We evolve the NS spin frequency $\omega = 2\pi/P$ and θ using Equations (11) and (12), with χ evaluated using Equation (2). Here, $M = 1.4\,M_\odot$, $R = 10^6$ cm, $B_{\rm p} = 10^{15}$ G, $P(0) = 1$ s, $\theta(0) = 20°$, $\psi = 10°$, and $\epsilon_{\rm eff} = 7.53 \times 10^{-7}$.

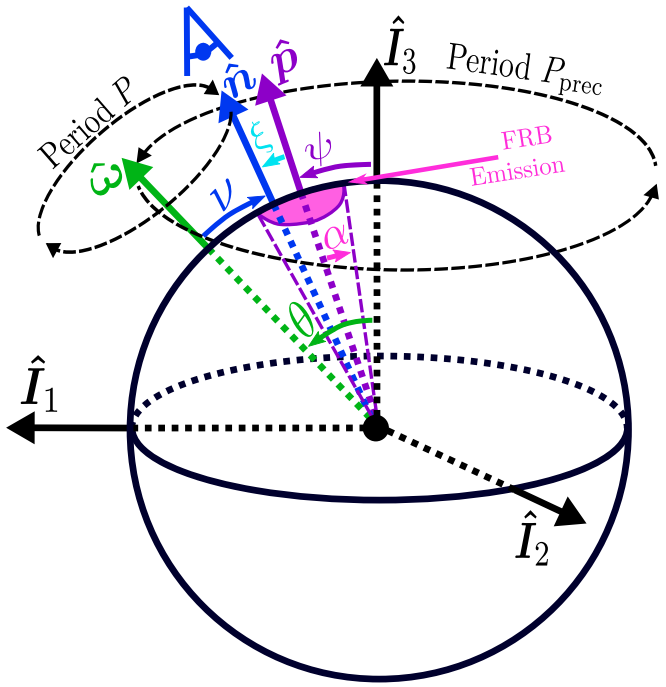

Figure 3. Geometric model of FRB emission from a precessing NS, depicted in the rotating frame (body frame) of the NS. See the text for details.

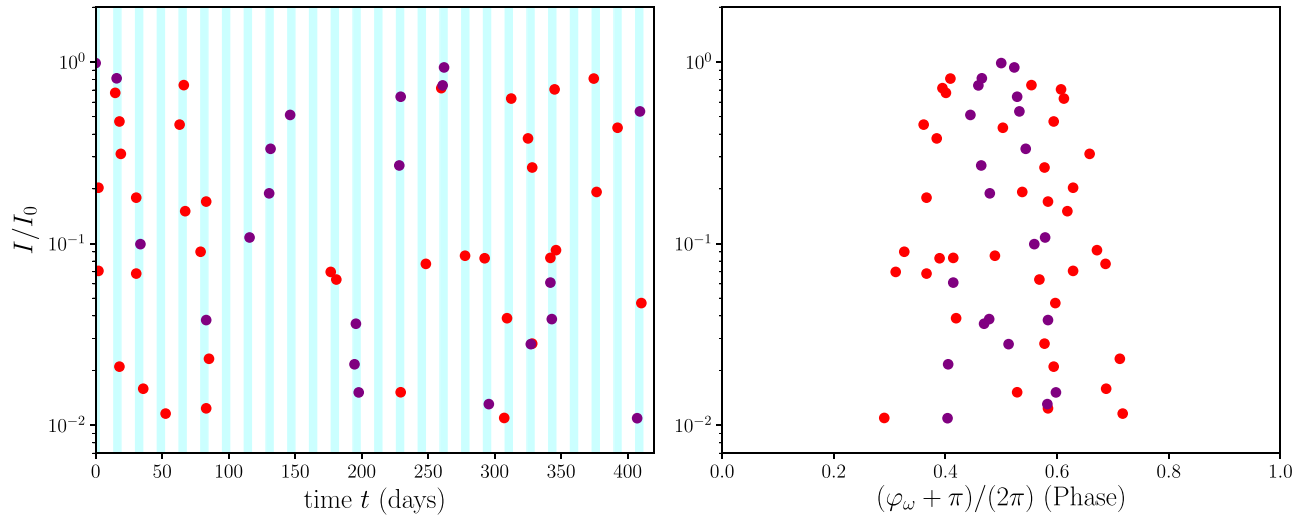

Figure 4. FRB emission I over time t (left panel) and precession phase φ_ω (Equation (3); right panel) for our precessing NS model over the observed duration of FRB 180916 ($t_{\rm obs} = 410$ days), with the spin precession frequency set to FRB 180916's period ($P_{\rm prec} = 16.35$ days). Dots show I evaluated at times t_i, while light cyan vertical bands denote ± 2.6 day intervals around multiples of $P_{\rm prec}$, which are the epochs where emission from FRB 180916 was detected. At every time $t = t_i$, the rotational phase φ_n (Equation (14)) is drawn randomly from the uniform interval $[0, 2\pi]$. The model parameters are $\psi = 3^\circ$ (red), $\psi = 7^\circ$ (purple), with $\theta = 10^\circ$, $\nu = \theta - \psi$, $\alpha = 1^\circ$, $N = 400$, and $\varphi_{\omega 0} = 0$. Our model assumes I_0 is fixed: all I variations with t are due to observing the FRB off-center ($\hat{\boldsymbol{n}} \neq \hat{\boldsymbol{p}}$; see Equation (15)).

the plane spanned by $\hat{\boldsymbol{I}}_1$ and $\hat{\boldsymbol{I}}_3$. The inclination between $\hat{\boldsymbol{n}}$ and $\hat{\boldsymbol{p}}$ is specified by the angle ξ ($\cos\xi = \hat{\boldsymbol{n}} \cdot \hat{\boldsymbol{p}}$). We consider a phenomenological emission model as an example, where we assume the radiation is emitted from a cone centered at $\hat{\boldsymbol{p}}$ with opening angle α, with the emission intensity I tapering off as $\hat{\boldsymbol{n}}$ becomes more misaligned with $\hat{\boldsymbol{p}}$:

$$I = I_0 \exp\left(-\frac{\xi^2}{2\alpha^2}\right). \tag{15}$$

Figure 4 shows two examples of the FRB emission pattern produced in our model. Although reproducing the periodicity of FRB 180916 requires $P_{\rm prec} = 16.35$ days, the NS spin period P and effective ellipticity $\epsilon_{\rm eff}$ remain unconstrained (but related; see Equation (4)). To leave P unconstrained, and to add stochasticity to our simple emission model, we evaluate $\hat{\boldsymbol{\omega}}(t)$ (Equation (2)) at N times ($N = 400$ for the example), which we denote by t_i, spread linearly between $t_1 = 0$ to $t_N = t_{\rm obs}$. We then pick $\varphi_n(t_i) = \varphi_i$ (Equation (14)) randomly from a uniform distribution over the interval $[0, 2\pi]$. The observer's orientation $\hat{\boldsymbol{n}}_i = \hat{\boldsymbol{n}}(t_i)$ is then evaluated with Equation (13), and the FRB emission I at time $t = t_i$ is computed with Equation (15).

We see from Figure 4 that, despite the simplicity of our model, it does well in reproducing the spacing of the periodic bursts, as well as the clustering of bursts over the precession phase. The left panel of Figure 4 shows some of the ± 2.6 day intervals around multiples of $P_{\rm prec}$ (light cyan bands) have no detectable bursts, while other epochs have multiple detectable bursts. More specifically, when $t/P_{\rm prec} \approx$ integer, some draws at times t_i get no instances of $\hat{\boldsymbol{n}}_i \approx \hat{\boldsymbol{p}}$, while other draws get multiple instances of $\hat{\boldsymbol{n}}_i \approx \hat{\boldsymbol{p}}$, due to the changing phase of $\hat{\boldsymbol{n}}$ around $\hat{\boldsymbol{\omega}}$. Notice that no bursts are detected at intervals away from integer multiples of $P_{\rm prec}$. This occurs because over most of the spin precession phase φ_ω, $\hat{\boldsymbol{\omega}}$ lies far from $\hat{\boldsymbol{p}}$, and $\hat{\boldsymbol{n}}$ closely follows $\hat{\boldsymbol{\omega}}$. The right panel of Figure 4 shows that the burst intensities I are clustered around the phase 0.5, with a spread that depends on the model parameters (angles ψ, θ, and ν; see Figure 3). Over this spread, the burst intensities vary by two orders of magnitude, with little dependence on φ_ω. All these features were seen in FRB 180916 (The CHIME/FRB Collaboration et al. 2020).

Figure 5 is the same as Figure 4, except instead of drawing a single value of the rotational phase φ_n at $t = t_i$, we pick N_n linearly spaced values spanning the interval $[0, 2\pi]$. With many more points sampled for φ_n, we see the FRB emission is confined to the light cyan epochs. The intensity profile shape with the FRB phase and the amount of clustering around phase 0.5 depend on the model parameters (ψ, θ, ν).

3. Polarization

In our simple model, the rotational frequency ω and the angles θ, ψ, and ν (see Figure 3) are constant over timescales much shorter than the spin-down time $t_{\rm sd}$ (Equation (10)), and thus the FRB emission pattern is constant. However, the magnetic obliquity χ (angle between $\hat{\boldsymbol{p}}$ and $\hat{\boldsymbol{\omega}}$) is modulated with period $P_{\rm prec}$. This can change the short-term (on the timescale of rotation period P) polarization pattern of the emission (e.g., Weisberg et al. 2010). In particular, if we use the rotating vector model to describe the linear polarization from the FRBs (e.g., Radhakrishnan & Cooke 1969; Wang et al. 2010; Lu et al. 2019), the shape of polarization sweep (as a function of the NS rotation phase) will be modulated with period $P_{\rm prec}$:

$$\mathrm{PA} = \tan^{-1}\left(\frac{-\sin\chi\sin\Psi}{\cos\chi\sin\nu - \sin\chi\cos\nu\cos\Psi}\right). \tag{16}$$

Here, PA is the polarization position angle (measured from the projection of $\hat{\boldsymbol{\omega}}$ in the sky plane), and Ψ is the rotational phase of the NS dipole axis $\hat{\boldsymbol{p}}$ around the rotation axis $\hat{\boldsymbol{\omega}}$. Figure 6 displays how the polarization angle PA is modulated by a precessing NS. Since we require the line of sight to be almost parallel to the dipole axis to observe FRB emission ($\hat{\boldsymbol{n}} \approx \hat{\boldsymbol{p}}$), a precessing NS can significantly affect the PA sweep across the rotational phase. Note that the "mean" polarization position angle (as determined by the projection of the rotation axis in the sky plane) is unchanged.

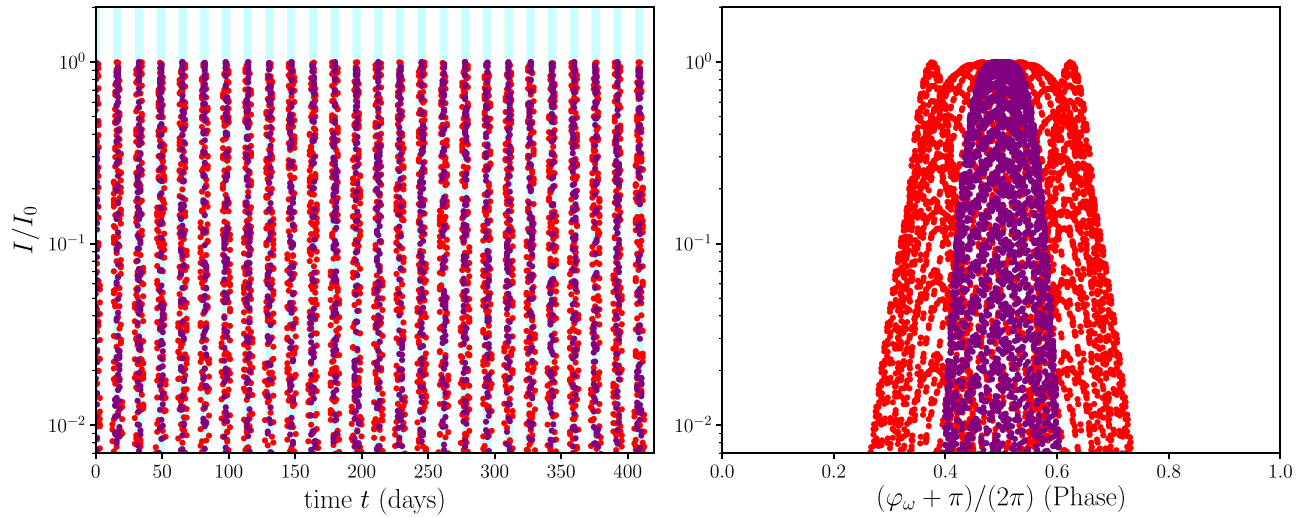

Figure 5. Same as Figure 4, except at every time $t = t_i$, we pick $N_n = 100$ linearly spaced values for the precession phase φ_n (Equation (3)) spanning the interval $[0, 2\pi]$.

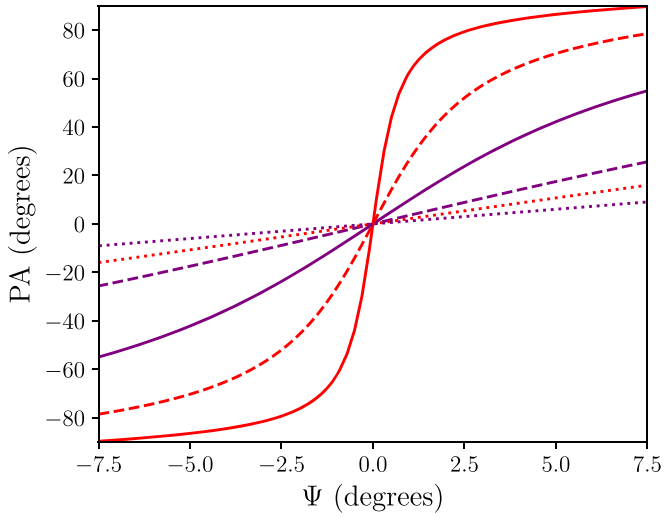

Figure 6. Position angle of polarization PA with rotational phase Ψ of $\hat{\boldsymbol{p}}$ around $\hat{\boldsymbol{\omega}}$, for $\varphi_\omega = 10^\circ$ (solid), $\varphi_\omega = 20^\circ$ (dashed), and $\varphi_\omega = 180^\circ$ (dotted). The model parameters are $\psi = 3^\circ$ (red) and $\psi = 7^\circ$ (purple), with $\theta = 10^\circ$ and $\nu = \theta - \psi$.

Over timescales comparable to or longer than the spin-down time, ψ remains constant (as we assume $\hat{\boldsymbol{p}}$ is frozen in the NS) and ν is also constant to a good precision (since $|\epsilon_{\rm eff}| \ll 1$), but ω and θ will decrease over time (see Figure 2). This will lengthen the NS precession period $P_{\rm prec}$ (Equation (4)) and induce a secular change in the magnetic obliquity χ (see Figure 2), which in turn will affect the polarization sweep.

4. Conclusions

We have shown that free precession of isolated neutron stars can in principle explain the observed 16 day periodicity of FRB 180916. The precession arises either from the aspherical deformation of the neutron star by strong internal magnetic fields or from the "effective" deformation associated with the near-zone dipole or multipole fields corotating with the star. The required field strength is of order 10^{15} G, depending on the dominant deformation mechanism (see Figure 1). Using a simple geometric FRB emission model, where radio bursts are emitted along the magnetic dipole axis, we show that the emission pattern from a precessing magnetar (Figures 3–5) can match that observed from FRB 180916. The fact that a stable precession period has been detected in FRB 180916 during 410 days of observation implies that the neutron star spin frequency ω satisfies $\omega R/c \ll 1$, i.e., the spin period is much larger than milliseconds, since a small spin period would lead to a rapidly changing FRB periodicity (Figure 2). Our simple model also predicts distinct variations in the polarization profiles for the FRB emission; these may be tested by future observations.

Needless to say, our simple geometric FRB emission model is highly idealized. Therefore the emission pattern and polarization profile presented in this Letter are for illustrative purposes only. But it is likely that any beamed emission that originates from inside a corotating magnetosphere will share qualitatively similar characteristics as our simple model.

We thank the anonymous referee, whose comments improved the clarity of this work. J.Z. thanks Dongzi Li, Ue-Li Pen, and Chris Thompson for useful discussions. This work was supported in part by NSF grant AST-17152. J.Z. is supported by a CITA postdoctoral fellowship.

ORCID iDs

J. J. Zanazzi https://orcid.org/0000-0002-9849-5886
Dong Lai https://orcid.org/0000-0002-1934-6250

References

Akgün, T., Link, B., & Wasserman, I. 2006, MNRAS, 365, 653
Arzamasskiy, L., Philippov, A., & Tchekhovskoy, A. e. 2015, MNRAS, 453, 3540
Baym, G., & Pines, D. 1971, AnPhy, 66, 816
Beloborodov, A. M. 2017, ApJL, 843, L26
Beskin, V. S., & Zheltoukhov, A. A. 2014, PhyU, 57, 799
CHIME/FRB Collaboration, Andersen, B. C., Bandura, K., et al. 2019, ApJL, 885, L24
Cordes, J. M., & Chatterjee, S. 2019, ARA&A, 57, 417
Cordes, J. M., & Wasserman, I. 2016, MNRAS, 457, 232
Cutler, C., Ushomirsky, G., & Link, B. 2003, ApJ, 588, 975
Davis, L., & Goldstein, M. 1970, ApJL, 159, L81
Goglichidze, O. A., & Barsukov, D. P. 2019, MNRAS, 482, 3032
Goldreich, P. 1970, ApJL, 160, L11
Katz, J. I. 2016, ApJ, 826, 226
Katz, J. I. 2018a, PrPNP, 103, 1

Katz, J. I. 2018b, MNRAS, 476, 1849
Kramer, M., Lyne, A. G., O'Brien, J. T., Jordan, C. A., & Lorimer, D. R. 2006, Sci, 312, 549
Landau, L. D., & Lifshitz, E. M. 1969, Mechanics (Oxford: Pergamon)
Levin, Y., Beloborodov, A. M., & Bransgrove, A. 2020, arXiv:2002.04595
Link, B., & Epstein, R. I. 1997, ApJL, 478, L91
Lu, W., & Kumar, P. 2018, MNRAS, 477, 2470
Lu, W., Kumar, P., & Narayan, R. 2019, MNRAS, 483, 359
Lyne, A., Graham-Smith, F., Weltevrede, P., et al. 2013, Sci, 342, 598
Lyubarsky, Y. 2014, MNRAS, 442, L9
Margalit, B., Berger, E., & Metzger, B. D. 2019, ApJ, 886, 110
Mastrano, A., Lasky, P. D., & Melatos, A. 2013, MNRAS, 434, 1658
Melatos, A. 1999, ApJL, 519, L77
Melatos, A. 2000, MNRAS, 313, 217
Munk, W. H., & MacDonald, G. J. F. 1975, The Rotation of the Earth: A Geophysical Discussion (Cambridge: Cambridge Univ. Press)
Petroff, E., Hessels, J. W. T., & Lorimer, D. R. 2019, A&ARv, 27, 4
Radhakrishnan, V., & Cooke, D. J. 1969, ApL, 3, 225
Sedrakian, A., Wasserman, I., & Cordes, J. M. 1999, ApJ, 524, 341
Shaham, J. 1977, ApJ, 214, 251
The CHIME/FRB Collaboration, Amiri, M., Andersen, B. C., et al. 2020, arXiv:2001.10275
Wang, C., Lai, D., & Han, J. 2010, MNRAS, 403, 569
Weisberg, J. M., Everett, J. E., Cordes, J. M., Morgan, J. J., & Brisbin, D. G. 2010, ApJ, 721, 1044
Zanazzi, J. J., & Lai, D. 2015, MNRAS, 451, 695
Zhang, Y. G., Gajjar, V., Foster, G., et al. 2018, ApJ, 866, 149